

Electronic and vibrational analysis of porphyrazine liquid-crystalline structure: Toward photochemical phase switching

David F. Dye, Krishnan Raghavachari, Jeffrey M. Zaleski *

Department of Chemistry, Indiana University, Bloomington, IN 47405, USA

Received 4 October 2007; accepted 28 October 2007

Available online 12 November 2007

Dedicated to Edward Solomon.

Abstract

The electronic and vibrational Raman spectra of octa-substituted ($R = -SC_{10}H_{21}$) Co- and Cu-porphyrazines are reported in their solid-state, mesophase, and isotropic liquid forms, as well as in THF solution. Their electronic spectra are composed of traditional Soret (CuS10 = 355 nm, CoS10 = 347 nm) and lower energy Q-bands (CuS10 = 669 nm, CoS10 = 639 nm), as well as a weaker, functionality-specific sulfur $n \rightarrow$ porphyrin π^* feature (CuS10 = 500 nm; CoS10 = 447 nm). In contrast to the broad Q-band for CoS10 in all three neat phases, the lower energy analogue for CuS10 is markedly sharper in the microcrystalline state, but similarly broadens in the mesophase, indicative of long range macrocycle π - π interactions that persist even into the liquid state. The resonance ($\lambda = 647$ nm) and off-resonance ($\lambda = 785$ nm) Raman spectra of these materials in each phase exhibit four diagnostic vibrations; the C_{α} - N_m stretch (~ 1540 – 1553 cm^{-1}), C_{β} - C_{β} stretch (~ 1450 cm^{-1}), C_{α} - C_{β} - N_p stretch (~ 1300 – 1315 cm^{-1}), and C_{α} - C_{β} stretch (~ 1070 cm^{-1}). For CoS10, these vibrations systematically shift to lower energy upon melting, while those for CuS10 collapse to degenerate sets. The differences in the electronic and vibrational profiles as a function of temperature suggest that the mesophase structure is governed by strong axial Co-S interactions for CoS10 which template macrocycle π - π stacking, while for CuS10 the same contacts exist, but they are phase dependent and markedly weaker. These inter-porphyrazine interactions are, therefore, responsible for the distinct differences in the melting and clearing temperatures of their respective mesophases. Finally, based on these diagnostic spectroscopic signatures, a photo-thermal, phase-switching mechanism is demonstrated with $\lambda = 785$ nm excitation at reduced temperatures, leading to the ability to spectrally monitor and phase change with a single photon source.

© 2007 Elsevier B.V. All rights reserved.

Keywords: Liquid crystal; Porphyrazines; Raman spectroscopy; Electronic absorption of liquid crystals

1. Introduction

The ability to generate a fluid, yet self-assembled, organized structure over long range with optical, magnetic, or conductive response have made liquid crystals (LC) an extremely valuable material for microelectronic devices such as electroluminescent displays of high uniformity [1], thermally-tunable semi-conductors [2,3], and thin-film optical photo-conductors [4–7]. The convergence of enhanced single molecule properties with controllable intermolecular

interactions via hybrid synthetic approaches has led to the development of selective materials that pervade applied electronics, most notably, organic rigid rod (calamitic) LCs that align in an electric field for technologically ubiquitous twisted nematic LC displays [8–11].

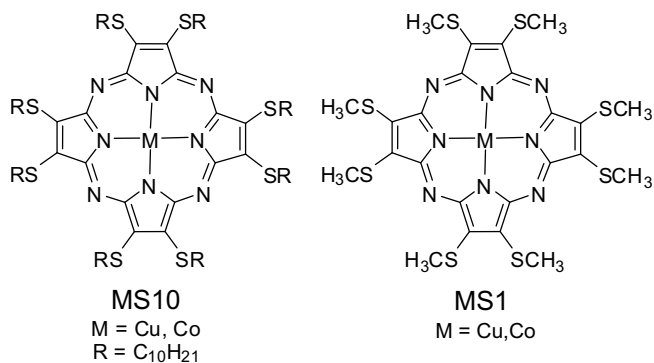
One of the challenges associated with control of LC behavior is the development of anisotropic, nanoscale segregation within a specific dimension [12]. To this end, discotic liquid crystalline materials that form columnar phases exhibit specific dimensionality and have found utility in self-ordering, micro-electronic components capable of behaving as uni-dimensional conductors/photo-conductors [7]. The typical molecular motif of these compounds

* Corresponding author. Tel.: +1 812 855 2134; fax: +1 812 855 8300.
E-mail address: zaleski@indiana.edu (J.M. Zaleski).

consists of an aromatic core which has been peripherally functionalized with long alkyl chains, resulting in columnar mesophases with core aromatic domains capable of behaving as charge carriers, surrounded by insulating alkyl chains that restrict charge transport to the columnar axis [13].

Although the conductivity and luminescent properties of organic LCs (e.g. discotics) is remarkable, by virtue of their closed-shell electronic structure, these materials are diamagnetic and require high external magnetic fields (~ 5 T) [1] to generate monodomains in which all mesophase columns are aligned over long range. Incorporation of open-shell metal ions into nanoscale-segregated, discotic architectures hybridizes the traditional mesomorphic character of discotics with tunable paramagnetism in both magnitude and directionality. This introduces the potential for facile magnetic alignment and switchable response at more modest external fields [14]. More broadly, metal ion incorporation into LC frameworks to form metallomesogens can also engender metal-mediated, chimeric electronic (e.g. conductivity) or geometric (e.g. enhanced rigidity) structural features that do not derive directly from the attributes of the individual components [15–17].

Octa(*n*-decylthio)-porphyrzine complexes of d^7 Co(II) and d^9 Cu(II) (CoS10, CuS10) are examples of paramagnetic, discotic LCs that form columnar mesophases at 62 and 69 °C, respectively, but exhibit disparate mesomorphic windows as defined by clearing points of 177 °C for CoS10, but only 122 °C for CuS10 [18].



The absence of a mesophase for the free-base derivative H₂S10, exemplifies the central role of the metal ion in mediating the liquid crystalline behavior of these porphyrzine metallomesogens via disparate intermolecular interactions within the columns. Moreover, the columnar mesophase domains of CoS10 can be aligned by relatively weak (~ 0.5 T) external magnetic fields due to the collinear paramagnetic and diamagnetic moments, while for CuS10, the paramagnetic moment along the *z*-axis competes directly with the perpendicular diamagnetic contribution of the macrocycle, thereby frustrating magnetic alignment of a monodomain [14]. Thus, for this class of discotic metallomesogens, substitution of the metal ion within the macrocycle can strongly modulate the long range order of the material by way of specific inter-macrocycle structural

interactions, as well as the electronic characteristics of the divalent central cation.

As a means to chemically define these inter-macrocycle interactions, we have taken advantage of the pronounced electronic spectral characteristics of these materials, as well as their resonance-enhanced and off-resonance Raman vibrational profiles to define the structural features of the crystalline, mesophase, and isotropic liquid states. The electronic spectra report on the degree of inter-macrocycle stacking [19–21], while specific frequency shifts in the vibrational features are diagnostic of the intermolecular interactions responsible for phase change [22–24]. These spectroscopic signatures are then correlated to explain the marked differences in the clearing points of CoS10 and CuS10. Finally, the intense electronic transitions exhibited by these materials afford an opportunity for introduction of thermal energy into liquid crystalline domains via photo-thermal heating, which permits remote phase switching of these materials while simultaneously monitoring these transitions via vibrational analysis.

2. Experimental

2.1. Sample preparation

Metalloporphyrzines were prepared according to methods previously described [14,18,25,26]. Sample integrities were confirmed by LDI- and FAB-MS, and elemental analysis.

2.2. Electronic absorption spectroscopy

Solution and neat electronic absorption spectra were obtained using a Perkin–Elmer Lambda 19 UV–Vis–NIR spectrometer. All solution data were recorded at ambient temperature. Neat samples were prepared via deposition of a drop (~ 5 mm) of a concentrated toluene solution of the sample on a quartz window. Solvent was allowed to evaporate at room temperature for a minimum of 30 min. prior to mounting in a copper cell for spectral analysis. Thermal excitation was performed by a 90 W heating element mounted within a 5" \times 1" copper cylinder in contact with the copper sample cell. Temperature was controlled using a Set-Temp Digital temperature controller (Laboratory Devices Inc.) with a K-type thermocouple mounted to the copper sample holder. Samples were heated to specific temperatures and allowed to equilibrate for approximately 5 min. prior to collection of spectra.

2.3. Raman spectroscopy

Off-resonance Raman spectra and images of samples were recorded using a Renishaw 1000B micro-Raman spectrometer equipped with a 785 nm SDL diode laser under variable power (0.2–20 mW) conditions. Temperature-dependent Raman spectra were obtained using a Linkam model TDS 600 variable temperature hot-state/cold-stage

assembly that was mounted directly on the Raman microscope.

Resonance Raman spectra were collected using $\lambda = 647.5$ nm laser excitation from a Coherent Innova 300 Kr⁺ ion laser. Backscattered light ($\sim 35^\circ$) was collected using a Nikon Nikkor AI-S 85 mm ($f/1.4$) camera lens and was focused through a depolarizer (CVI) onto the entrance slit of a custom-built, $f/4$ subtractive-mode, double monochromator equipped with 600 grooves/mm (500 nm blaze) gratings. Output of this filter stage was focused on the entrance slit of an Acton Spectrapro 500i spectrometer ($f/6.5$) operating with a 1200 grooves/mm (750 nm blaze) grating. The dispersed scattering was recorded using a back-illuminated, liquid N₂ cooled charge coupled device (Princeton Instruments) with a 30 mm \times 14.4 mm active area (2500 \times 600 pixel array). Solution spectra were measured in spinning, thin-walled, 5 mm glass NMR tubes. Neat spectra were collected by depositing powdered samples on the surface of a quartz window backed by a copper slug mounted in the custom heating element used for variable temperature electronic spectroscopy.

2.4. Computational methods and vibrational analysis

To understand the electronic structures of the different species, computational studies were performed using density functional theory with the standard B3LYP hybrid functional. We utilized the 6-31+G(d,p) basis set (containing a set of spd diffuse functions along with f-polarization functions) on Co and Cu, and the 6-31G(d,p) basis set (containing d-type polarization functions on C, N, and S, and p-polarization functions on H) to optimize the molecular geometries and to obtain the harmonic vibrational frequencies and the associated Raman intensities. Both structures minimize in C_4 symmetry with alternating methyl groups located above and below the molecular plane. The calculated vibrational frequencies (gas phase) were scaled uniformly by a factor of 0.982, and resulted in very good overall agreement between the computed and experimental ($\lambda_{\text{exc}} = 785$ nm, THF solution) values. All calculations were performed with the GAUSSIAN-03 [27] program suite.

3. Results and discussion

3.1. Electronic structure

The solution electronic absorption spectra of CuS10 and CoS10 (Fig. 1a) are dominated by two distinct transitions typical of metalloporphyrazine architectures [28,29]: a high energy Soret band (CuS10 = 355 nm, CoS10 = 347 nm) and a low energy Q-band (CuS10 = 669 nm, CoS10 = 639 nm) showing a vibronic overtone to higher energy ($\nu \sim 1250$ cm⁻¹) [29]. An additional feature arising from a $n_{\text{sulfur}} \rightarrow \pi^*$ transition is apparent at $\lambda \sim 500$ nm for CuS10 and 447 nm for CoS10, which is in general agreement with the electronic absorption spectra reported for

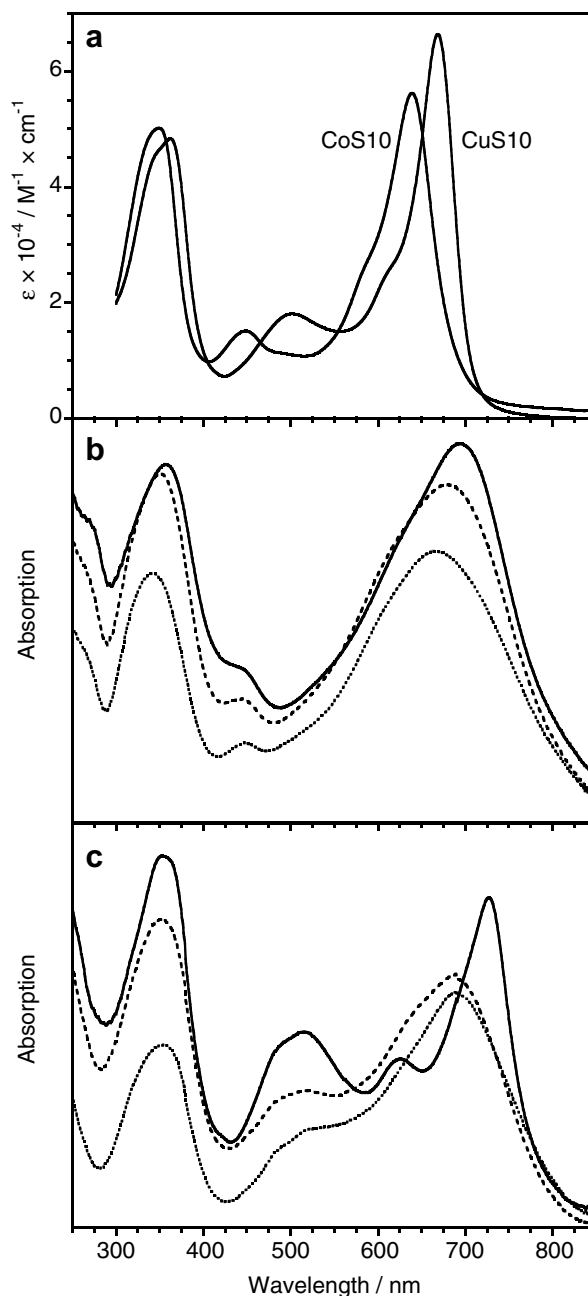


Fig. 1. Electronic absorption spectra for MS10 compounds. (a) THF solution (14.6 μ M CuS10, 15.1 μ M CoS10), (b) CoS10 and (c) CuS10 at 20 °C (—), 100 °C (---), and 200 °C (···).

MS1 compounds [19,25,26]. The blue-shift of the CoS10 spectral features relative to CuS10 is common to other metallo-porphyrin and porphyrazine frameworks, and is related to the relative hardness of the central ion [29].

For CoS10 in the solid state (Fig. 1b), this general electronic structure is retained, though substantial broadening of the Q-band from a full-width, half-max (FWHM) of ~ 1200 cm⁻¹ in solution to ~ 4000 cm⁻¹ in the solid state, and a red-shift from of $\lambda = 639$ nm (solution) to 690 nm (solid) are observed ($\Delta \sim 1150$ cm⁻¹). Both the broadening [19,21] and red-shift [20] can be attributed to increased π -stacking of the porphyrazine macrocycles that manifests

over long range. Heating neat CoS10 to its mesophase (100 °C) results in a slight blue-shift of the Q- (19 nm) and Soret bands (6 nm), but no significant changes in the linewidths are observed. Similarly, when CoS10 is heated past the clearing point, the Q- and Soret bands further blue-shift (6 and 10 nm, respectively) while maintaining their bandwidths. This indicates that the intermolecular structure for CoS10 is maintained in all three phases, but the degree of π -stacking is systematically relaxed, as evidenced by the blue-shift of the Q and Soret bands.

In contrast, the neat electronic absorption spectrum of CuS10 demonstrates distinct differences in macroscopic structure upon transition from crystalline to mesophase and isotropic liquid (Fig. 1c). Unlike CoS10, the solid-state absorption profile of CuS10 retains the general characteristics of the solution spectrum with respect to the Soret and $n_{\text{sulfur}} \rightarrow \pi^*$ transitions, but the Q-band shows substantial variability between these spectra. As a solid, the Q-band red-shifts to $\lambda = 726 \text{ nm}$ ($\Delta = 1170 \text{ cm}^{-1}$) relative to THF solution, but unlike CoS10, CuS10 maintains a narrow bandwidth (FWHM $\sim 1100 \text{ cm}^{-1}$). The shift to lower energy can be readily explained by intermolecular π -interactions between macrocycles as shown for crystallographically characterized Cu-thiadiazole porphyrazines, which exhibit a 3.2 Å inter-planar separation [30]. The lack of significant broadening of the Q-band despite the presence of π -interactions may be related to a lower degree of long-range π -stacking in the solid. Of note is the sharpness of the low-energy side of the Q-band relative to the broadened, high-energy slope, indicating the presence of an unresolved vibrational component of the Q-band underlying the solid-state spectrum. A higher energy transition is also apparent at $\lambda = 624 \text{ nm}$, which is not directly observed in solution. This feature has been reported previously [31], however a thorough discussion of the assignment has not been presented. Our results suggest that the origin of the $\lambda = 624 \text{ nm}$ band may derive from small, asymmetric molecular distortion upon crystallization, introducing distinct Q_x and Q_y transitions which are reminiscent of those observed for free-base thioalkyl porphyrazines [19,32–35]. The π -nature of the transition is consistent with resonance Raman enhancement of core macrocycle ring modes upon $\lambda = 647 \text{ nm}$ excitation. Additionally, in contrast to the $\sim 1250 \text{ cm}^{-1}$ energy gap between the parent and vibrational component of Q-band, which derives from a combination of macrocycle ring modes [29], the separation of the Q_x and Q_y symmetry partners is typically greater, on the order of 3000 cm^{-1} . The observed 2250 cm^{-1} separation of the Q-bands for crystalline CuS10 is significantly larger than expected for the vibrational components of a Q-band, and thus may derive from a decrease in molecular symmetry upon crystallization.

Upon heating to the mesophase, the Q-band broadens significantly (FWHM $\sim 3300 \text{ cm}^{-1}$) and shows a pronounced blue-shift to $\lambda = 686 \text{ nm}$ ($\Delta = 800 \text{ cm}^{-1}$), which encompasses the previously resolved higher energy feature. Since the mesophase allows in-plane rotation of the por-

phyrazine macrocycle within the liquid crystal columnar order, averaging of Q_x and Q_y asymmetry occurs upon melting, and the spectra now exhibit extended π -stacking as observed for CoS10. Heating past the clearing point does not further change the shape or energy of the electronic transitions in CuS10. Therefore, the mesophase and isotropic electronic absorption spectra of CuS10 reveal extended order consistent with that observed for CoS10 throughout its phases. The clear blue-shift upon melting indicates that the crystal packing responsible for the change in electronic structure of solid CuS10 has been relaxed in the higher temperature phases. Thus, though disparate crystal packing energies are predicted to be responsible for the observed initial melting points of CoS10 and CuS10, the predominant intermolecular forces present in the mesophases of each system should be similar, indicating that the differences in observed clearing points must be, in general, the result of weaker inter-macrocycle interactions within CuS10 mesophase columns relative to CoS10.

It has been shown that substitution of the central metal ion of porphyrazines can have a strong influence on the crystal packing scheme of otherwise identical macrocycles [30]. Indeed, powder diffraction studies of CoS10 and CuS10 reveal that they exhibit different space groups in the solid-state, though detailed structural information is not available due to extensive disordering in the microcrystalline samples examined [14]. For analogous octakis(ethylthio)porphyrazines (MS2), the observed crystal packing for CoS2 exhibits a herringbone pattern dictated by sulfur lone-pair donation to the half-occupied $d(z^2)$ orbital of the central cobalt ion of an adjacent macrocycle [36]. It is of note that the *meso*-nitrogen shows no distortion from the macrocycle plane in this X-ray structure, indicating that M–S bonding directs the lone pair parallel to the adjacent macrocycle where it has little interaction with the neighboring π -system. Unfortunately, no crystallographically characterized copper thioalkyl porphyrazines exist for comparison. However, it is apparent based on the distinct electronic absorption features for crystalline CuS10 that this crystal packing motif may not be translated upon substitution of the central metal ion. For crystalline CuS10, the additional electron density in the $d(z^2)$ orbital would be expected to lead to a Jahn–Teller distorted, filled–filled axial interaction in pure C_4 symmetry with one of the sulfur lone pairs in the solid-state structure, leading to no axial interaction and only weak intermolecular association.

For structurally characterized metallo-thiadiazole porphyrazines containing metal ions that strongly bind axial ligands (e.g. Co^{2+} , Zn^{2+} , and Fe^{2+}), crystal packing is typically dictated by axial interactions with lone pairs from thiadiazole nitrogen atoms of adjacent macrocycles [30]. Conversely, for copper thiadiazole porphyrazines, the Jahn–Teller distortion and the accompanying lack of, or elongation of, axial bonds results in a crystalline structure in which π – π interactions are maximized at the expense of axial association. The resulting macroscopic structure reveals porphyrazine units that typically pack with *meso*-

nitrogen atoms from adjacent molecules non-covalently capping the central copper ion [30]. In the case of CuS10, the presence of sp^3 sulfur lone pairs from the periphery side-chains may lead to an additional weak-axial interaction with the Cu-center upon transition to the mesophase, in which sulfur coordination causes the macrocycle π – π interactions to slip slightly as is the case for CoS10. This hypothesis is consistent with the observation that all MS10 metalloporphyrazines highlighted above exhibit a mesophase, but the free-base derivative does not. The weaker axial interaction for CuS10 vs. CoS10 is also manifested in the more pronounced blue-shift of the Q-band in the mesophase and isotropic liquid states.

3.2. Vibrational analysis

A comparison between the resonance Raman spectra of the solution, crystalline, *meso*- and isotropic phases of CoS10 and CuS10 (Fig. 2) shows distinct changes in both the energy and asymmetry of several molecular vibrations upon solvation and melting. Subsequent heating of these metalloporphyrazines past their clearing temperatures shows no additional spectral change of significance. The

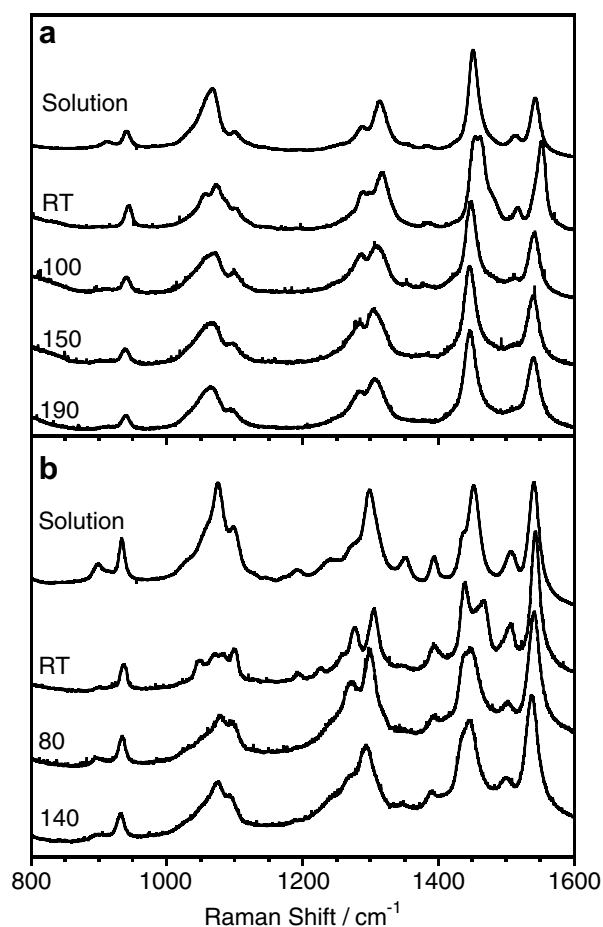


Fig. 2. Resonance Raman spectra ($\lambda_{\text{exc}} = 647.5 \text{ nm}$) of THF solution (RT), solid, *meso*- and isotropic phases of: (a) CoS10 and (b) CuS10. Temperatures are given in $^{\circ}\text{C}$.

resonance Raman spectra of CoS10 exhibit systematic vibrational shifts to lower energy upon phase change, whereas the spectra of CuS10 simplify upon melting as sets of vibrations collapse to form fewer distinct signatures due to increased molecular symmetry and averaging. Most notable are the modes in both at ~ 1075 , ~ 1300 , ~ 1450 , and $\sim 1540 \text{ cm}^{-1}$. Although a normal mode analysis of the vibrational structure of assorted porphyrazines and phthalocyanines has been performed [37–40], a specific investigation of thioalkyl porphyrazines has not been previously reported. Since the vibrational structure of a porphyrazine will be perturbed by the addition of electron rich sulfur to the periphery of the macrocycle through mixing of the sulfur lone pairs into the π -system, we have undertaken a computational analysis of the vibrational structure of CoS10 and CuS10. To minimize computational time, MS10 molecules were modeled as MS1, preserving the core macrocycle structure and influence of the thioalkyl groups while minimizing the difficulties of reaching a geometric minimum for flexible $-\text{C}_{10}\text{H}_{21}$ *n*-decyl chains. Though the alkyl chains of the thioalkylporphyrazines have a strong influence on their liquid crystalline behavior [18,19,41], the vibrational structures of these compounds are dominated by in-plane macrocycle distortions, allowing our model to accurately elucidate the specific normal modes associated with the observed vibrations.

Comparison of calculated MS1 and measured MS10 Raman spectra (Table 1) show good agreement for both CoS10 and CuS10. The solution spectra correlate within 21 cm^{-1} for all predominant vibrations; the only exception is the $\text{C}_{\alpha}\text{-N}_m$ stretch which exhibits a substantially greater deviation ($\Delta_{\text{CoS10}} = 50 \text{ cm}^{-1}$, $\Delta_{\text{CuS10}} = 35 \text{ cm}^{-1}$) from the gas phase computation. This is not surprising since the exposed *meso*-nitrogen lone pair is sensitive to the external chemical environment, and may serve as a reporter of periphery structure intrusion. Between CoS10 and CuS10, the intensity and energy of many observed solution vibrations are different, but there is a high degree of conservation of the $\text{C}_{\alpha}\text{-N}_m$, $\text{C}_{\beta}\text{-C}_{\beta}$, $\text{C}_{\beta}\text{-C}_{\alpha}\text{-N}_p$, and $\text{C}_{\alpha}\text{-C}_{\beta}$ stretches (Fig. 3), which are the most diagnostic of phase change.

The $\text{C}_{\alpha}\text{-N}_m$ stretches at 1552 cm^{-1} for crystalline CoS10 and 1543 cm^{-1} for CuS10 (Fig. 2) show a disparate but discernible shift to lower energy upon solvation in THF ($\Delta_{\text{CoS10}} = 10 \text{ cm}^{-1}$, $\Delta_{\text{CuS10}} = 3 \text{ cm}^{-1}$), which is expected since the exposed lone pair of the *meso*-nitrogens should be quite sensitive to molecular environment. A similar shift occurs for neat CoS10 upon melting from the solid to the mesophase ($100 \text{ }^{\circ}\text{C}$), with no additional energy change observed upon heating past the clearing point. Conversely, for neat CuS10, the $\text{C}_{\alpha}\text{-N}_m$ vibration shows little shift in energy upon heating through the mesophase or past the clearing point.

For the CoS10 $\text{C}_{\beta}\text{-C}_{\beta}$ stretch ($\nu = 1453 \text{ cm}^{-1}$), shifts comparable to those described for $\text{C}_{\alpha}\text{-N}_m$ are observed; once again, the energy of the vibration is decreased upon solvation and melting. Since it is expected that the sulfur adjacent to the β -carbon directs the crystal packing of

Table 1
Comparison of select calculated (C_4 symmetry) and observed Raman ($\lambda_{\text{exc}} = 785 \text{ nm}$, THF solution) vibrations

Assignment	Calculated symmetry	CoS1			CuS10		
		Calc. (cm^{-1})	Obs. (cm^{-1})	Diff.	Calc. (cm^{-1})	Obs. (cm^{-1})	Diff.
$C_{\alpha}\text{-N}_m$ stretch	B	1592	1542	50	1578	1543	35
$C_{\alpha}\text{-N}_m/C_{\beta}\text{-C}_{\beta}$ stretch	A	1529			1516		
$C_{\alpha}\text{-N}_m\text{-C}_{\alpha}$ stretch	A	1512	1505	7	1491	1512	-21
$C_{\beta}\text{-C}_{\beta}$ stretch	A	1474			1461		
$C_{\beta}\text{-C}_{\beta}$ stretch	B	1465	1453	12	1458	1452	6
$C_{\alpha}\text{-N}_m\text{-C}_{\alpha}$ bend/ $C_{\alpha}\text{-N}_p\text{-C}_{\alpha}$ bend	A	1396	1395	1	1392	1382	10
$C_{\beta}\text{-C}_{\alpha}\text{-N}_p$ stretch	B	1316	1301	15	1300	1315	-15
Pyrrole breathing	B	1109	1100	9	1110	1107	3
$C_{\alpha}\text{-C}_{\beta}$ stretch	B	1083	1076	7	1081	1070	11
C-H ₃ tilt	B	989			989		
$C_{\alpha}\text{-N}_m\text{-C}_{\alpha}$ bend	B	931	935	-4	923	940	-17
$C_{\alpha}\text{-N}_m\text{-C}_{\alpha}$ rock	B	760	757	3	754	759	-5
S-CH ₃ stretch	E	680			680		
Macrocycle breathing	A	587	598	-11	584	600	-14

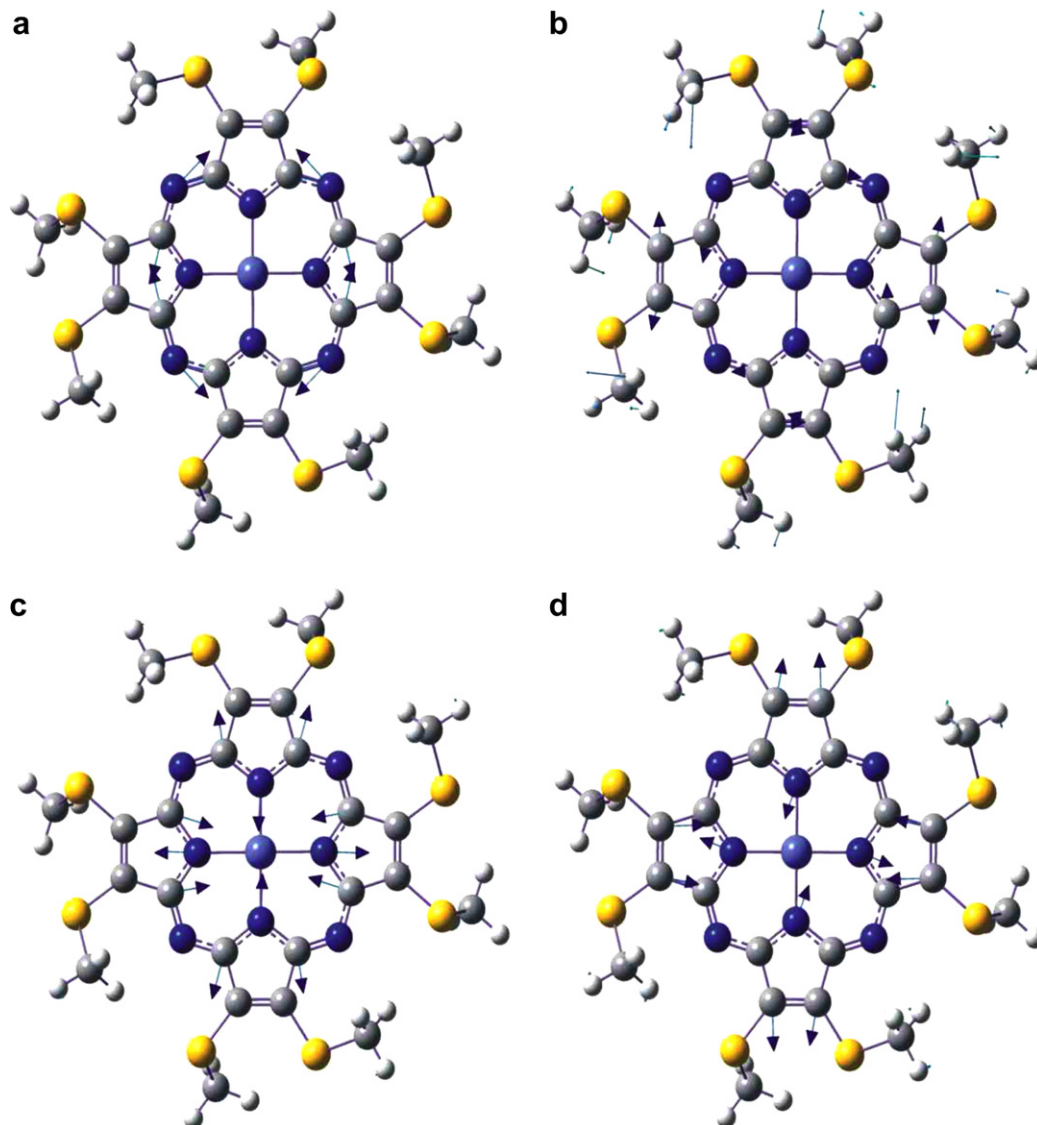


Fig. 3. Calculated molecular vibrations for CoS1 (C_4 symmetry): (a) $C_{\alpha}\text{-N}_m$ stretch (1592 cm^{-1}), (b) $C_{\beta}\text{-C}_{\beta}$ stretch (1465 cm^{-1}), (c) $C_{\alpha}\text{-C}_{\beta}\text{-N}_p$ stretch (1316 cm^{-1}), and (d) $C_{\alpha}\text{-C}_{\beta}$ stretch (1083 cm^{-1}).

CoS10, it follows that vibrations associated with this carbon should shift to lower energy once the axial metal–sulfur interaction is relaxed upon transition to the mesophase. In contrast, for crystalline CuS10, two distinct C_{β} – C_{β} vibrations are apparent that subsequently collapse into a single observed feature ($\nu = 1452 \text{ cm}^{-1}$) upon solvation and melting. Since no strong axial metal–sulfur interaction is expected for CuS10 in the crystalline phase, an ensemble of near-degenerate vibrations arises from slight structural asymmetry caused by π -interaction with an adjacent macrocycle in the solid state, resulting in observation of distinct C_{β} – C_{β} stretching modes. A similar degeneracy-lifting asymmetry is observed for the C_{β} – C_{α} – N_p and C_{α} – C_{β} vibrations of crystalline CuS10, which also show frequency collapse upon solvation or melting. This behavior is not observed in these vibrations for CoS10 upon phase change, indicating that the π -mediated asymmetry responsible for generating the splitting of the CuS10 vibrations is not operative for CoS10.

Off resonance ($\lambda_{\text{exc}} = 785 \text{ nm}$) Raman spectra taken in 10°C increments with emphasis on the C_{α} – N_m , C_{β} – C_{β} , and C_{β} – C_{α} – N_p vibrations more clearly show these trends (Fig. 4). Once again, the Raman spectra indicate that the primary vibrations of CoS10 shift to lower energy upon warming, whereas the features observed for crystalline CuS10 exhibit multiple signatures for the same in-plane normal mode that collapse upon phase change. Consistent with this observation, the computed vibrational profile reveals two nearly degenerate C_{β} – C_{β} vibrations which are not resolved in the $\lambda = 785 \text{ nm}$ solution spectrum, but due to crystal packing effects, are individually detected for multiple C_{β} – C_{β} sites in the solid-state Raman profile.

Apparent in both the CoS10 and CuS10 off-resonance Raman spectra are phase changes at temperatures (-30 to -10°C for CoS10 and 40 to 60°C for CuS10) lower than expected based on the established melting points of these materials due to laser-induced, photo-thermal heating of the samples. For the temperatures through which melting occurs, the observed spectra are an addition of the crystalline and mesophase profiles arising from incomplete melting due to the non-uniform laser beam profile over the photolyzed area resulting in uneven heating of the sample. For CoS10, the appearance of spectral features correlating to the mesophase begins at -30°C , with complete phase change apparent by -10°C . This can be seen clearly for the C_{α} – N_m vibration in which a low energy shoulder from the mesophase CoS10 begins to emerge at -30°C , finally dominating and remaining unchanged at -10°C . For CuS10, the multiplicity of the C_{β} – C_{β} and C_{β} – C_{α} – N_p stretches in crystalline CuS10 are preserved through the heating ramp up to 30°C , past which broadening is apparent (40 – 60°C) and finally, a single isotropic feature is observed. The lower laser-induced phase transition temperature for CoS10 relative to CuS10 is not a chemical phenomenon, but rather derives from the difference in laser excitation power density used for collection of each data set (CoS10: 1.9 mW ; CuS10: 0.19 mW).

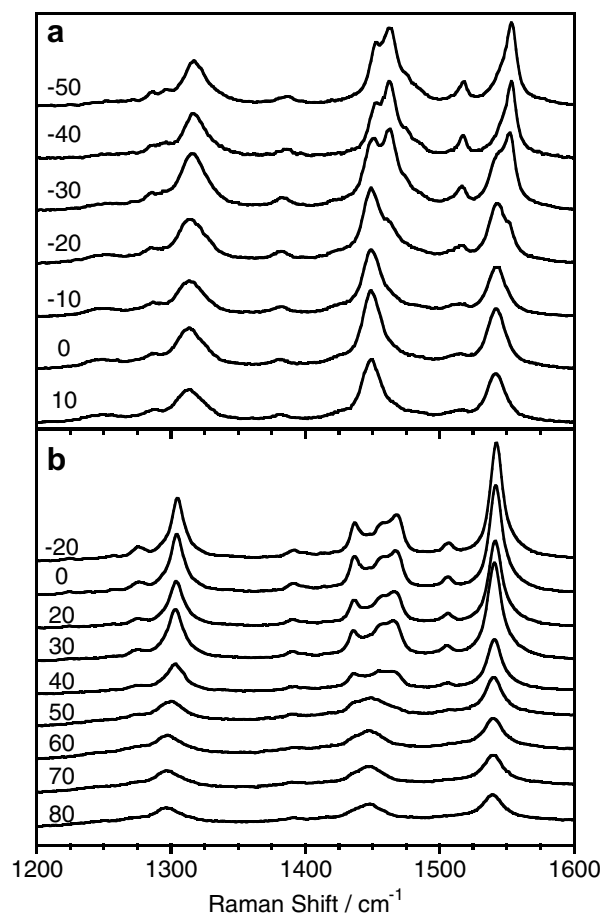


Fig. 4. Temperature-dependent, off-resonance Raman spectra of: (a) CoS10 (1.9 mW , $\lambda_{\text{exc}} = 785 \text{ nm}$) and (b) CuS10 (0.19 mW , $\lambda_{\text{exc}} = 785 \text{ nm}$) during phase change from solid to liquid-crystal. Temperatures are given in $^\circ\text{C}$.

3.3. Proposed structures

Based on the electronic and vibrational data, and in conjunction with structurally characterized metalloporphyrazines, we propose the models for CoS10 and CuS10 inter-macrocycle interactions in the solid state illustrated in Fig. 5. For CoS10, a crystalline structure strongly directed by the preservation of axial Co–S interactions is consistent with the observed preference for cobalt metalloporphyrazines to crystallize in order to maximize axial Co–S bonding with available lone pairs of adjacent molecules [30,36]. Furthermore, this crystalline orientation forces π overlap between adjacent molecules, which is reflected in minimal perturbation of the electronic structure between solid, mesophase, and isotropic liquid states. The physical picture is also supported by Raman data in which crystalline CoS10 exhibits shifts for the C_{β} – C_{β} vibration consistent with sulfur interactions between adjacent porphyrazine units which are maintained, but relaxed upon melting. The shift to lower energy of the C_{α} – N_m vibration in the mesophase and isotropic liquid mandates that the CoS2 *meso*-nitrogen in the crystalline state is not effectively

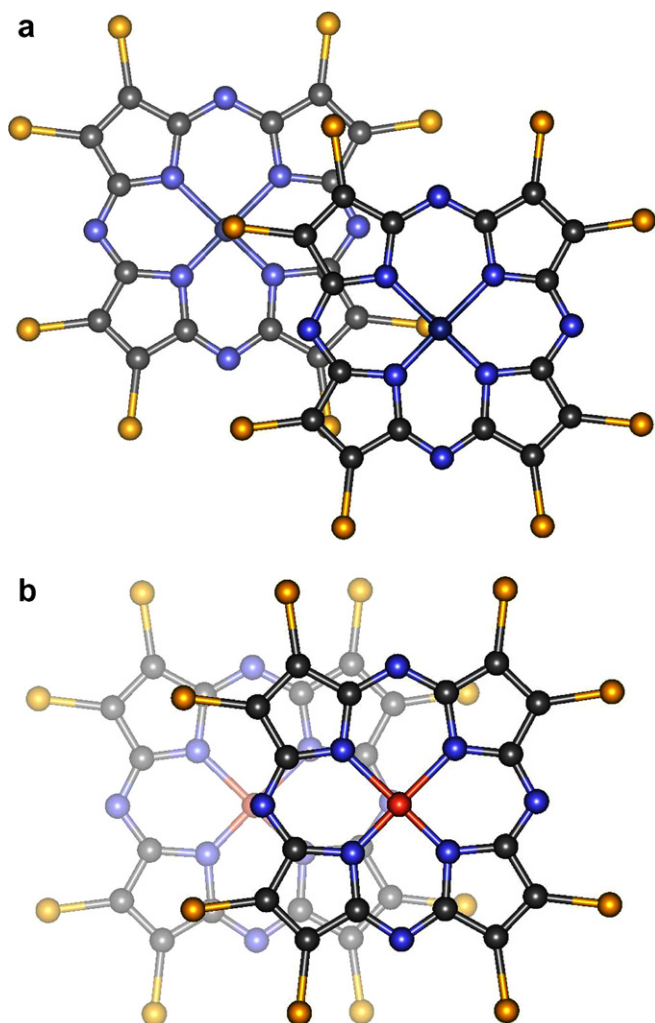


Fig. 5. Proposed crystal packing for: (a) CoS10 and (b) CuS10. Alkyl chains have been omitted for clarity.

interacting with protons from side-chains on the adjacent macrocycles due to their Co–S mediated ring displacement. This restriction is relieved upon transition to the meso-phase, which permits free rotation of the macrocycles within the columns. The enhanced degrees of freedom allow the side-chains to sample the void above/below the *meso*-nitrogen of the adjacent macrocycle leading to weak H-bonding with the C–H bond of the side-chain (Fig. 6a). Dynamic, inter-columnar breathing enhances this effect in the mesophase resulting in the marked shift to lower energy of the C_{α} – N_m vibration analogous to solvation effects by THF.

In contrast, we propose that the order of CuS10 in the crystalline state is dictated by maximizing overlap between adjacent π -frameworks. Copper metalloporphyrinoids generally do not mediate strong axial bonding interactions in the solid state, and are instead observed to crystallize in motifs that maximize facial π interactions between macrocycles [30]. Extension of this crystal would produce two distinct molecular axes due to the asymmetric distortion of the macrocyclic π system, which is evident in the electronic

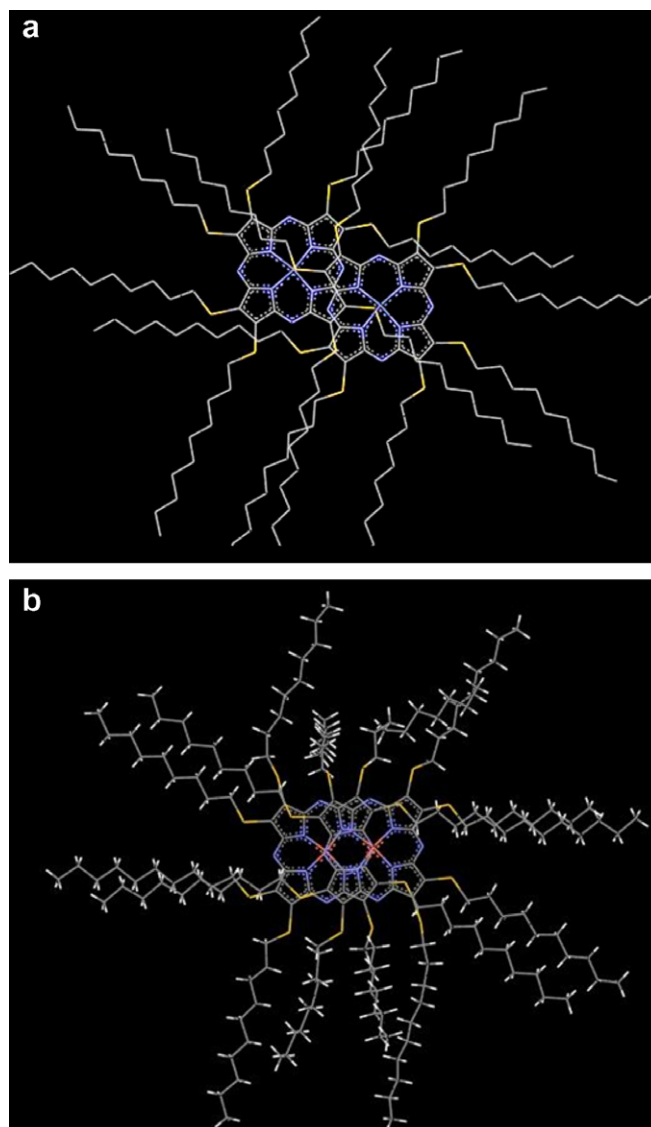


Fig. 6. Proposed model of inter-macrocycle and side-chain interactions for: (a) CoS10, and (b) CuS10. The non-slipped orientation for CuS10 in the solid-state illustrates the ability of the side chains to sample the void space in the vicinity of the *meso*-nitrogen lone-pair of the adjacent macrocycle.

absorption spectrum of the microcrystalline material. Similarly, the strong π overlap will generate disparate energies for the pyrrole-centered vibrations, as observed in the crystalline Raman spectra for CuS10. Such a structure also places the thioalkyl chains in position to fill the void adjacent to the *meso*-nitrogen of the partner macrocycle, effectively solvating the lone-pair and leading to minimal shift in the C_{α} – N_m vibration across the phases relative to THF solution (Fig. 6b). Upon melting, relaxation of this π overlap will relieve the distorted C_{β} – C_{β} and C_{β} – C_{α} – N_p vibrational components making them nearly degenerate, and leading to a blue-shift of the Q-band as observed in Raman and electronic spectra, respectively, of CuS10 in the meso-phase and isotropic liquid. The accompanying broadening of the electronic spectrum, and its similarity to that of

CoS10 in these phases, suggests that CuS10 must adopt a weak but definable Cu–S interaction upon melting that leads to long range order and liquid crystallinity. Thus, the stronger axial interaction for CoS10 ultimately gives rise to a higher clearing temperature and broader mesophase relative to CuS10.

3.4. Photo-induced switching

To explore the photo-induced phase-switching potential of these liquid crystalline structures, a series of CuS10 spectra were collected at room temperature using incrementally increasing excitation powers (Fig. 7). Photolysis at low laser power (0.2 mW/60 s exposure) generates the typical Raman vibrational profile with no indication of phase change in the sample either through visual microscopic inspection or shifts in vibrational energies. Increasing the laser power to 2 mW leads to immediate broadening of the spectral features and minor frequency shifts indicative of the onset of melting to the mesophase, along with subtle visual changes in phase at the very center of the sample photolysis area. Due to the larger illumination area, the Raman spectral profile is a mixture of solid-state and mesophase vibrational features. Upon increasing the laser power to 5 mW, melting is visually detectable, and is accompanied by complete transformation of the spectrum to that observed for mesophase CuS10 (c.f. Fig. 4b). Further photolysis at higher powers (10, 20 mW) produces only small additional perturbations in the observed spectra at 600 and 1315 cm^{-1} , as well as between 1050 and 1100 cm^{-1} .

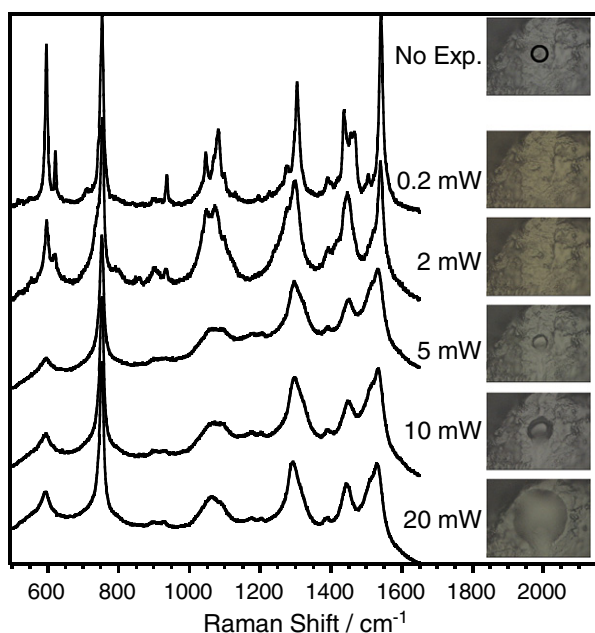


Fig. 7. Raman spectra ($\lambda_{\text{exc}} = 785 \text{ nm}$) of CuS10 as a function of increasing laser excitation powers. Images showing the degree of sample melting resulting from photolysis were recorded following spectral collection. An image of the sample prior to laser exposure with relative laser spot size are shown for comparison.

However, images of the sample reveal a more prominent change in sample phase as evidenced by the larger melt area. At 10 mW, the center of image begins to show transition to the isotropic liquid, while the perimeter of the melt area remains liquid crystalline in nature based on the strong similarity of the 5 and 10 mW Raman profiles. At an excitation power of 20 mW, the entire area being sampled converts to the isotropic liquid, and the corresponding Raman spectra reflect the transition by slight spectral sharpening of the bands at 600, 1070, and 1315 cm^{-1} . This power dependence of phase, accompanied by a diagnostic spectral signature, suggests a potential utility for metalloporphyrazine liquid crystals in optical, phase-switching applications.

4. Conclusion

Electronic and Raman spectra of CoS10 and CuS10 porphyrazines in solid, mesophase, isotropic liquid, and THF solution reveal π – π inter-macrocycle interactions that in the mesophase and isotropic liquid are influenced by axial metal interactions with the sulfur of an adjacent macrocycle. For CoS10, these interactions are considerable stronger than for CuS10, as evidenced by the enhanced blue-shift in the electronic spectra for the latter in the mesophase. Accompanying the stacking is a disparate solvation of the *meso*-nitrogen derived from the alkyl side-chain filling the void and hydrogen bonding with the in-plane sp^2 lone pair. The orientation of the π -stacked macrocycles for CoS10 do not allow this to occur in the solid state, but rather require dynamic ring and chain motion in the mesophase to relieve the restriction. In contrast, for CuS10, we propose that this hydrogen bonding occurs in the solid-state and is maintained through the phases, explaining the lack of a prominent shift in the C_α – N_m vibration. Finally, the ability of the large porphyrazine chromophore to non-radiatively decay optical energy to heat permits photo-thermal phase switching of these materials. In this way, a single laser source can be used to both stimulate and monitor vibrational signatures of each phase via in situ Raman. Methodology of this type may prove useful for the fundamental development of photo- or magneto-optical materials.

Acknowledgements

We would like to thank Dr. Brian Pate for synthesizing the metalloporphyrazines, and Glen Ferguson for assistance generating figures of the normal modes. The support of Merck & Co., Inc. (D.F.D.) is gratefully acknowledged.

References

- [1] S.H. Eichhorn, A. Adavelli, H.S. Li, N. Fox, Mol. Cryst. Liq. Cryst. 397 (2003) 347.
- [2] S. Chandrasekhar, S.K. Prasad, Contemp. Phys. 40 (1999) 237.

- [3] K. Ohta, K. Hatsusaka, M. Sugibayashi, M. Ariyoshi, K. Ban, F. Maeda, R. Naito, K. Nishizawa, A.M. van de Craats, J.M. Warman, *Mol. Cryst. Liq. Cryst.* 397 (2003) 325.
- [4] B. Blanzat, C. Barthou, N. Tercier, J.J. Andre, J. Simon, *J. Am. Chem. Soc.* 109 (1987) 6193.
- [5] R.J. Bushby, O.R. Lozman, *Curr. Opin. Solid State Mater. Sci.* 6 (2003) 569.
- [6] L.K. Chau, E.J. Osburn, N.R. Armstrong, D.F. O'Brien, B.A. Parkinson, *Langmuir* 10 (1994) 351.
- [7] D. Markovitsi, I. Lecuyer, J. Simon, *J. Phys. Chem.* 95 (1991) 3620.
- [8] W. Hall, J. Hollingshurst, J.W. Goodby, *Handb. Liq. Cryst. Res.* (1997) 17.
- [9] H. Hirschmann, V. Reiffenrath, *Handb. Liq. Cryst.* 2A (1998) 199.
- [10] Y. Owechko, *Handb. Liq. Cryst. Res.* (1997) 505.
- [11] M. Schadt, *Annu. Rev. Mater. Sci.* 27 (1997) 305.
- [12] T. Kato, N. Mizoshita, K. Kishimoto, *Angew. Chem., Int. Ed.* 45 (2006) 38.
- [13] S. Kumar, *Chem. Soc. Rev.* 35 (2006) 83.
- [14] B.D. Pate, S.-M. Choi, U. Werner-Zwanziger, D.V. Baxter, J.M. Zaleski, M.H. Chisholm, *Chem. Mater.* 14 (2002) 1930.
- [15] L. Oriol, M. Pinol, J.L. Serrano, *Prog. Polym. Sci.* 22 (1997) 873.
- [16] K. Praefcke, A. Eckert, *Mol. Cryst. Liq. Cryst.* 396 (2003) 265.
- [17] M.B. Ros, *Metallomesogens* (1996) 419.
- [18] F. Lelj, G. Morelli, G. Ricciardi, A. Roviello, A. Sirigu, *Liq. Cryst.* 12 (1992) 941.
- [19] S. Belviso, G. Ricciardi, F. Lelj, *J. Mater. Chem.* 10 (2000) 297.
- [20] M. Kasha, H.R. Rawls, M.A. El-Bayoumi, *Pure Appl. Chem.* 11 (1965) 371.
- [21] W.I. White, in: D. Dolphin (Ed.), *The Porphyrins: Physical Chemistry, Part C*, Academic Press, New York, 1978, p. 303.
- [22] M.G. Giorgini, A. Arcioni, G. Venditti, M. Musso, *J. Raman Spectrosc.* 38 (2007) 78.
- [23] N. Hayashi, A. Kocot, M.J. Linehan, A. Fukuda, J.K. Vij, G. Heppke, J. Naciri, S. Kawada, S. Kondoh, *Phys. Rev. E: Stat., Nonlinear, Soft Matter Phys.* 74 (2006) 051706/1.
- [24] D.S. Kang, K.-S. Kwon, S.I. Kim, M.-S. Gong, S.S.A. Seo, T.W. Noh, S.-W. Joo, *Appl. Spectrosc.* 59 (2005) 1136.
- [25] P. Doppelt, S. Huille, *New J. Chem.* 14 (1990) 607.
- [26] C.J. Schramm, B.M. Hoffman, *Inorg. Chem.* 19 (1980) 383.
- [27] G.W.T.M.J. Frisch, H.B. Schlegel, G.E. Scuseria, M.A. Robb, J.R. Cheeseman, J.A. Montgomery, Jr., T. Vreven, K.N. Kudin, J.C. Burant, J.M. Millam, S.S. Iyengar, J. Tomasi, V. Barone, B. Mennucci, M. Cossi, G. Scalmani, N. Rega, H.N.G.A. Petersson, M. Hada, M. Ehara, K. Toyota, R. Fukuda, J. Hasegawa, M. Ishida, T. Nakajima, Y. Honda, O. Kitao, H. Nakai, M. Klene, X. Li, J.E. Knox, H.P. Hratchian, J.B. Cross, C. Adamo, J. Jaramillo, R. Gomperts, R.E. Stratmann, O. Yazyev, A.J. Austin, R. Cammi, C. Pomelli, J.W. Ochterski, P.Y. Ayala, K. Morokuma, G.A. Voth, P. Salvador, J.J. Dannenberg, V.G. Zakrzewski, S. Dapprich, A.D. Daniels, M.C. Strain, O. Farkas, D.K. Malick, A.D. Rabuck, K. Raghavachari, J.B. Foresman, J.V. Ortiz, Q. Cui, A.G. Baboul, S. Clifford, J. Cioslowski, B.B. Stefanov, G. Liu, A. Liashenko, P. Piskorz, I. Komaromi, R.L. Martin, D.J. Fox, T. Keith, M.A. Al-Laham, C.Y. Peng, A. Nanayakkara, M. Challacombe, P.M.W. Gill, B. Johnson, W. Chen, M.W. Wong, C. Gonzalez, J.A. Pople, Gaussian, Inc., Pittsburgh, PA, 2003.
- [28] E.J. Baerends, G. Ricciardi, A. Rosa, S.J.A. van Gisbergen, *Coord. Chem. Rev.* 230 (2002) 5.
- [29] M. Gouterman, in: D. Dolphin (Ed.), *The Porphyrins: Physical Chemistry, Part A*, Academic Press, New York, 1978.
- [30] Y. Suzuki, M. Fujimori, H. Yoshikawa, K. Awaga, *Chem. Eur. J.* 10 (2004) 5158.
- [31] F. Bonosi, G. Ricciardi, F. Lelj, G. Martini, *J. Phys. Chem.* 97 (1993) 9181.
- [32] G. Morelli, G. Ricciardi, A. Roviello, *Chem. Phys. Lett.* 185 (1991) 468.
- [33] G. Ricciardi, F. Lelj, F. Bonosi, *Chem. Phys. Lett.* 215 (1993) 541.
- [34] F. Bonosi, G. Ricciardi, F. Lelj, G. Martini, *J. Phys. Chem.* 98 (1994) 10613.
- [35] C.F. van Nostrum, F.B.G. Benneker, N. Veldman, A.L. Spek, A.-J. Schouten, R.J.M. Nolte, *Recl. Trav. Chim. Pays-Bas* 113 (1994) 109.
- [36] G. Ricciardi, A. Rosa, I. Ciofini, A. Bencini, *Inorg. Chem.* 38 (1999) 1422.
- [37] T.V. Basova, B.A. Kolesov, A.G. Gurek, V. Ahsen, *Thin Solid Films* 385 (2001) 246.
- [38] D. Braun, A. Ceulemans, *J. Phys. Chem.* 99 (1995) 11101.
- [39] R. Aroca, Z.Q. Zeng, J. Mink, *J. Phys. Chem. Solids* 51 (1990) 135.
- [40] D.R. Tackley, G. Dent, W.E. Smith, *Phys. Chem. Chem. Phys.* 3 (2001) 1419.
- [41] D.M. Knawby, T.M. Swager, *Chem. Mater.* 9 (1997) 535.